

THE TULLY-FISHER RELATION OF BARRED GALAXIES

STÉPHANE COURTEAU¹

Department of Physics and Astronomy, University of British Columbia, 6224 Agricultural Road, Vancouver, BC V6T 1Z1, Canada;
courteau@astro.ubc.ca

DAVID R. ANDERSEN¹

Max-Planck-Institut für Astronomie, Königstuhl 17, D-69117 Heidelberg, Germany; andersen@mpia-hd.mpg.de

MATTHEW A. BERSHADY

Department of Astronomy, University of Wisconsin–Madison, 475 North Charter Street, Madison, WI 53706;
mab@astro.wisc.edu

LAUREN A. MACARTHUR¹

Department of Physics and Astronomy, University of British Columbia, 6224 Agricultural Road, Vancouver, BC V6T 1Z1, Canada;
lauren@astro.ubc.ca

AND

HANS-WALTER RIX

Max-Planck-Institut für Astronomie, Königstuhl 17, D-69117 Heidelberg, Germany; rix@mpia-hd.mpg.de

Received 2002 December 2; accepted 2003 April 27

ABSTRACT

We present new data exploring the scaling relations, such as the Tully-Fisher relation (TFR), of bright barred and unbarred galaxies. A primary motivation for this study is to establish whether barredness correlates with, and is a consequence of, virial properties of galaxies. Various lines of evidence suggest that dark matter is dominant in disks of bright *unbarred* galaxies at 2.2 disk scale lengths, the point of peak rotation for a pure exponential disk. We test the hypothesis that the Tully-Fisher (TF) plane of barred high surface brightness galaxies is offset from the mean TFR of unbarred galaxies, as might be expected if barred galaxies are “maximal” in their inner parts. We use existing and new TF data to search for basic structural differences between barred and unbarred galaxies. Our new data consist of two-dimensional $H\alpha$ velocity fields derived from SparsePak integral field spectroscopy and V - and I -band CCD images collected at the WIYN Observatory² for 14 strongly barred galaxies. Differences may exist between kinematic and photometric inclination angles of barred versus unbarred galaxies. These findings lead us to restrict our analysis to barred galaxies with $i > 50^\circ$. We use WIYN/SparsePak (two-dimensional) velocity fields to show that long-slit (one-dimensional) spectra yield reliable circular speed measurements at or beyond 2.2 disk scale lengths, far from any influence of the bar. This enables us to consider line width measurements from extensive TF surveys that include barred and nonbarred disks and derive detailed scaling relation comparisons. We find that for a given luminosity, barred and unbarred galaxies have comparable structural and dynamical parameters, such as peak velocities, scale lengths, and colors. In particular, the location of a galaxy in the TF plane is independent of barredness. In a global dynamical sense, barred and unbarred galaxies behave similarly and are likely to have, on average, comparable fractions of luminous and dark matter at a given radius.

Subject headings: galaxies: formation — galaxies: kinematics and dynamics — galaxies: photometry — galaxies: spiral — galaxies: structure — stellar dynamics

On-line material: color figures

1. INTRODUCTION

Based on the flatness of rotation curves in spiral galaxies and the density profiles inferred from X-ray temperatures and stellar velocity dispersion profiles in ellipticals, it is widely believed that galaxies are embedded in nondissipative massive dark halos. More than 90% of the total mass of a galaxy would be in the form of dark matter. Less appreciated is the fact that we still have a rather muddled picture of the mass distribution of luminous and dark matter in the

luminous part of a galaxy. This is unfortunate, since the final distribution of baryons in a galaxy is a telltale sign of its formation and evolution. Numerical and analytical models of disk formation in a dissipationless dark matter halo predict, for realistic total fractions of baryonic to dark matter, that spiral disks should live in dark halos that dominate the mass fraction at nearly all radii (see, e.g., Mo, Mao, & White 1998), beyond about a disk scale length. This ratio may quite possibly be different for barred and unbarred galaxies of a given total mass or luminosity (Courteau & Rix 1999, hereafter CR99).

Recent debates about the cold dark matter (CDM) paradigm (see, e.g., Weinberg & Katz 2002; Sellwood 2003) and galaxy structural properties inferred from new infrared surveys (see, e.g., Eskridge et al. 2002; MacArthur, Courteau, & Holtzman 2003) have brought barred galaxies

¹ Visiting Astronomer, Kitt Peak National Observatory, National Optical Astronomy Observatory (NOAO). The NOAO is operated by the Association of Universities for Research in Astronomy (AURA), Inc., under cooperative agreement with the National Science Foundation.

² The WIYN Observatory is a joint facility of the University of Wisconsin–Madison, Indiana University, and the NOAO.

to the fore. Bar perturbations in galaxies, far from just being dynamical curiosities, actually play a fundamental role in shaping galaxies into the structures we see today (see Buta, Crocker, & Elmegreen 1996 for reviews). For instance, the early dynamical evolution of a massive, rapidly rotating, gaseous bar could provide enough energy and angular momentum to significantly modify the inner CDM halo (Silk 2002). Dynamical and structural studies of barred galaxies are, however, few, in part because of the complexity in interpreting their velocity fields (see, e.g., Weiner, Sellwood, & Williams 2001) and their surface brightness profiles (see, e.g., MacArthur et al. 2003). Many large-scale flow studies of spiral galaxies have also excluded disturbed or barred galaxies to minimize scatter, as previously believed, in the distance-measuring technique. The latter studies have enabled extensive scaling relation studies of unbarred galaxies, but little attention has been paid to their barred cousins. This is, again, deplorable, as a comparative study of the scaling relations for barred and unbarred galaxies would potentially unravel clues about the structure and origin of bars and the role of dynamical processes in establishing the Hubble sequence of disk galaxies.

The body of numerical simulations of barred galaxies is comparatively richer and has recently reached new heights with the availability of superior N -body realizations with more than 10^6 particles (post-2010 readers may enjoy a moment of laughter). Until just recently, it was believed that bar instabilities in a disk might be suppressed by a massive halo. Thus, only low-concentration halos, or equivalently, systems of very high surface brightness (HSB) or low angular momentum per unit luminosity, would be prone to generating a nonaxisymmetric (bar/oval) structure in their center (Ostriker & Peebles 1973; accounts of the misconceptions surrounding this argument are presented in Bosma 1996 and Sellwood & Evans 2001).

The suggestion that barred galaxies would have an especially high ratio of baryons to dark matter within the optical disk (“maximal disk”) might imply that these systems define their own sequence in the luminosity–line width diagram, if one assumes that unbarred galaxies are, on average, submaximal (CR99). Thus, for a given absolute magnitude, a galaxy with higher baryon fraction, or disk mass-to-light (M/L) ratio, would have a shorter disk scale length and rotate faster. Verification of this important, although tentative, suggestion should be easily obtained from a large sample of uniformly selected barred galaxies that are part of a well-calibrated, self-consistent luminosity–line width survey. The current study was largely motivated by this question.

In discussing the mass distribution in spiral galaxies, we use the definition that a disk is maximal if it contributes more than 75% of the total rotational support of the galaxy at $R_{\text{disk}} \equiv 2.2h_{\text{disk}}$, the radius of maximum disk circular speed (Sackett 1997). Thus, for a maximal disk, $V_{\text{disk}}/V_{\text{total}} \gtrsim 0.75$, where V_{total} is the total amplitude of the rotation curve (RC) at R_{disk} and $V_{\text{disk}} = V(R_{\text{disk}})$. Note that for $V_{\text{disk}}/V_{\text{total}} = 0.7$, the disk and halo contribute equally to the potential at R_{disk} . Large bulges for late-type galaxies make little difference for the computation of this quantity at R_{disk} (CR99).

The pattern speeds of bars have been considered as a potential indicator of the relative fraction of dark matter in galaxy disks. N -body simulations of bar formation in stellar

disks suggest that dynamical friction from a dense dark matter halo dramatically slows the rotation rate of bars in a few orbital periods (Debattista & Sellwood 1998, 2000, the latter hereafter DS00). Because bars are observed to rotate quickly, DS00 proposed that dark matter halos in HSB galaxies must have a low central density; thus, their disks ought to be maximal. These simulations were revisited by Valenzuela & Klypin (2003, hereafter VK03) with similar N -body simulations (no gas) but with an order-of-magnitude improvement in the force resolution. VK03 found that dynamical friction from transfer of angular momentum of the bar to the halo does play a role but, contrary to DS00, that that effect appears to be small. In addition, VK03 find that bars can form even in the presence of strong halos and that stellar disks make a negligible contribution to the inner RC (at R_{disk}). The bars modeled in DS00 also span nearly the entire disk, whereas the observed bar-to-disk scale length ratio seldom exceeds 1.5, as also pointed out by VK03. These authors find that mass and force resolution are critical for modeling the dynamics of bars, and the contentious results from DS00 would stem primarily from numerical resolution effects. However, the higher force resolution of VK03 induces numerical viscosity, which may bring their results into question (J. Sellwood 2003, private communication). Free from the vagaries of numerical simulations, Athanassoula (2003) uses analytical calculations to warn against the use of bar slowdown rate to set limits on the baryonic-to-dark matter fraction within the optical radius.³ This work confirms that bars in halos need not get slowed down efficiently and that bars can and do exist in subdominant halos.

A complete picture of bar dynamics awaits a self-consistent treatment of both the stars *and* the gas embedded in a cosmologically motivated halo. These simulations should include dynamical friction and ultimately reproduce the fraction of strong bars detected in the infrared and predict the rate of bar slowdown and dissolution as a function of bulge/total brightnesses, time, and environment.

The model-independent quest of the relative matter distribution in barred and unbarred galaxies is by no means straightforward either, but it is most significant, as it provides a necessary constraint for the shape and amplitude of the dark matter density profile in the luminous part of a galaxy. Whether disks are maximal or not at R_{disk} , the inner 1–2 kpc may be dominated by baryons in most galactic systems, including early and late-type HSB barred and unbarred spiral galaxies (see, e.g., Broeils & Courteau 1997; Corsini et al. 1999), low surface brightness (LSB) galaxies (Swaters 1999; Swaters, Madore, & Trewhella 2000; Fuchs 2003), and elliptical galaxies (see, e.g., Brighenti & Mathews 1997; see also Ciotti 2000). Maximally massive disks in LSB galaxies may, however, require unrealistically high disk M/L ratios (Swaters et al. 2000; Fuchs 2003), based on stellar population synthesis models.

Also troublesome is our lack of knowledge about the distribution of matter in our own Milky Way. Whether it has a maximal disk (Gerhard 2002) or not (Dehnen & Binney 1998; Klypin, Zhao, & Somerville 2002) is still a matter of debate. Crucial elements for local mass density

³ Athanassoula (2003) finds that the bar slowdown rate depends not only on the relative halo mass at a given radius, but also on the velocity dispersion of both the bulge and disk components.

estimates include the precise contribution of the massive central bar (see, e.g., Zhao, Rich, & Spergel 1996), or elongated bulge (Kuijken 1995), an accurate measure of the disk scale length, and constraints from microlensing toward the bulge.

The determination of the relative fraction of visible and dark matter in external barred and unbarred galaxies relies on our ability to determine stellar M/L ratios accurately. The modeling of disk dynamical mass in barred galaxies relies heavily on the interpretation of the nonaxisymmetric motions of ionized gas around the bar within the context of a hydrodynamical model. This model does have a local potential, and hence the bar and disk M/L ratios are parameters of the model. It is certainly a more complicated approach than using collisionless particles as dynamical tracers, as with stellar velocity dispersions, but the latter has its own complications as well (see, e.g., Swaters et al. 2003). Significant improvements in mass-modeling techniques for individual galaxies are expected with the development of stellar population synthesis models (Bell & de Jong 2001) and dynamical constraints (Weiner et al. 2001), to yield realistic M/L ratios, and further constraints from cosmological simulations of dark halos, to curtail disk-halo degeneracies (A. Dutton et al. 2003, in preparation).

Various lines of circumstantial evidence for external systems favor dark matter halos that dominate the mass budget within R_{disk} . Arguments based on the stellar kinematics of galactic disks (Bottema 1997), gas kinematics (Kranz, Slyz, & Rix 2003), the stability of disks (Fuchs 2001), and the lack of correlated scatter in the Tully-Fisher relation (hereafter TFR; Tully & Fisher 1977) of unbarred LSB and HSB galaxies (CR99) suggest that, *on average*, disks with $V_{\text{max}} < 200 \text{ km s}^{-1}$ are submaximal. The two very different analyses by Bottema and CR99 both yield $V_{\text{disk}}/V_{\text{total}} = 0.6 \pm 0.1$, or $M_{\text{dark}}/M_{\text{total}} = 0.6 \pm 0.1$, for HSB galaxies at R_{disk} . The geometry of gravitational lens systems, coupled with RC measurements, can also be used to decompose the mass distribution of a lensing galaxy. This promising technique, pioneered by Maller et al. (2000), has been applied to the galaxy-lens system 2237+0305 by Trott & Webster (2002), who find $V_{\text{disk}}/V_{\text{total}} = 0.57 \pm 0.03$, in excellent agreement with the studies above and predictions from analytical models of galaxy formation (see, e.g., Dalcanton, Spergel, & Summers 1997; Mo et al. 1998).

While a consistent picture of galaxy structure is emerging, in which a dark halo dominates with $M_{\text{dark}}/M_{\text{total}} \geq 0.6$ well into the optical disk, a number of pro-maximal disk arguments are still found in the literature, citing evidence from the shapes and extent of RCs and mass modeling (see, e.g., Bosma 2002). The match between *pure-disk* mass models and $H\alpha$ RCs (see, e.g., Broeils & Courteau 1997; Seljak 2002; Jimenez, Verde, & Oh 2003) is usually satisfactory for spiral galaxies of different surface brightnesses and morphologies and has often been invoked as evidence for a maximal concentration of baryons relative to the dark matter inside the optical disk (Buchhorn 1992; Palunas & Williams 2000). However, mass modeling with $H\alpha$ RCs alone is not a uniquely determined problem. The equivalence of, or degeneracy between, the two descriptions—pure disk versus submaximal disk+dark halo—was demonstrated in Broeils & Courteau (1997) and CR99 for a sample of 300 disk galaxies; residuals for the maximal and submaximal fits are indistinguishable. Without an accurate estimate of M/L_{disk} or external constraints on $V_{\text{disk}}/V_{\text{virial}}$ at

R_{disk} , mass modeling cannot disentangle maximal and submaximal disk models.

Our study of the dynamical structure of barred and unbarred galaxies will offer new insights in the debate over the maximal disk hypothesis in barred and unbarred galaxies. However, we plan to revisit this controversial issue in a future presentation (S. Courteau et al. 2003a, in preparation). Rather, we pursue our comparison of barred and unbarred galaxies in the context of global scaling relations.

1.1. Available Galaxy Samples

The study of scaling relations of barred galaxies and tracing their location in the TFR require that we utilize “fundamental plane” surveys of an ensemble of galaxies. The “Shellflow” and “SCII” all-sky Tully-Fisher (TF) surveys of Courteau et al. (2000) and Dale et al. (1999) are useful in that respect. These surveys were designed to map the convergence of the velocity field on $\sim 60 h^{-1}$ Mpc scales while minimizing calibration errors between different telescopes in different hemispheres; state-of-the-art TF calibrations are thus available in both cases. Both surveys include line width and luminosity measurements for a small fraction of barred galaxies that can be used to study structural trends, provided that the presence of the bar does not bias these measurements. More details about the surveys are given in § 3.

In order to calibrate existing long-slit spectra of barred galaxies and initiate a comprehensive study of barred galaxy velocity fields, we have collected new deep V - and I -band images and integral field $H\alpha$ velocity fields of 14 strongly barred galaxies at the WIYN 3.5 m telescope. We present the new data and velocity field analysis in § 2 and discuss possible limitations of the data, such as those due to inclination uncertainties and noncircular motions. We then examine the location of barred and unbarred galaxies in the TF samples discussed above in § 3. We find that barredness does not play a role in the luminosity–line width and luminosity-size planes of spiral galaxies. In § 4, we discuss future programs that may benefit the study of scaling relations in barred and unbarred galaxies.

2. A NEW WIYN SURVEY OF BARRED GALAXIES

2.1. Observations

In 2002 March, we obtained two-dimensional $H\alpha$ velocity maps and deep V - and I -band photometry at the WIYN 3.5 m (3 nights) and 0.9 m (2 nights) telescopes, respectively, for 14 strongly barred bright galaxies (SBb–SBc; $m_B \lesssim 15$; see Table 1) and one unbarred spiral galaxy (NGC 3029). The galaxies were selected according to the same criteria as the TF Shellflow survey of spiral galaxies, save the emphasis on the barlike morphology. Ultimately, we aim to calibrate our new data on the same system as Shellflow, a survey deficient in barred galaxies, to enable direct comparisons between barred and unbarred systems.

Integral field spectroscopy (IFS), which is lacking in Shellflow and SCII, is required to fully characterize the velocity amplitudes of the bulge, bar, and underlying disk, especially if noncircular velocities are conspicuous. We have obtained two-dimensional velocity maps with the SparsePak integral field unit (IFU; M. A. Bershadsky et al. 2003a, in preparation). The SparsePak IFU is a fiber optic array of 82 fibers mounted at the Nasmyth f/6.3 focus imaging port on the WIYN 3.5 m telescope. SparsePak has 75 fibers

TABLE 1
VELOCITY FIELD AND STRUCTURAL PARAMETERS

ID	Type	N	i_{kin} (deg)	i_{phot} (deg)	PA_{kin} (deg)	PA_{phot} (deg)	v_a (km s $^{-1}$)	r_l (arcsec)	β	γ	R_{bar} (arcsec)	h_{disk} (arcsec)	v_0 (km s $^{-1}$)
IC 0784	SAB(rs)bc	79	71	...	286	...	191.3	3.32	-0.48	1.70	4863.1
IC 2104	(R')SB(s)bc	114	64	63	106	107	395.0	9.64	0.91	0.44	31.6	11.5	5513.2
NGC 2540	SB(rs)cd: H II	118	50	55	127	124	166.8	2.98	-0.02	1.17	6.6	8.7	6317.0
NGC 3029	SAB(r)c	98	39	48	240	242	128.2	3.69	-0.25	1.48	...	7.9	6586.6
NGC 3128	SB(s)b?	111	74	72	349	366	214.1	7.58	0.14	1.20	16.8	16.5	4639.4
NGC 3469	(R')SB(r)ab	87	45	45	308	326	174.4	1.13	3.01	2.17	14.8	12.8	4645.8
NGC 3832	SB(rs)bc	159	26	34	155	120	88.8	9.56	-0.05	2.21	14.9	15.4	6904.2
NGC 4999	SB(r)b	171	35	36	124	123	226.6	4.36	0.00	1.10	19.8	14.3	5627.6
NGC 5504 ^a	SAB(s)bc	136	<18	43	302	322	111.7	6.29	0.03	1.25	20.5	12.7	5223.8
UGC 4416	SB(s)b	169	64	61	165	168	198.6	10.36	0.14	1.40	26.6	16.1	5544.4
UGC 5141	SBbc	129	44	56	1	3	189.1	1.98	-0.90	10.31	11.9	8.6	4984.9
UGC 6895	SAB(rs)bc	194	44	47	189	189	231.1	5.40	0.09	20.68	...	29.3	6364.6
UGC 7173	SB(rs)b LINER	96	36	38	239	224	194.7	6.53	-0.23	12.60	11.1	13.4	6800.1
UGC 8229	SB(r)b	83	41	56	34	57	166.2	0.37	0.00	1.14	20.2	9.7	5982.5
UGC 8241	SB(rs)bc starburst	142	<8	23	202	220	56.2	0.71	1.94	2.85	20.0	9.5	5603.2

^a The photometric parameters for NGC 5504 come from V -band imaging.

arranged in a sparsely filled grid subtending an area of $72'' \times 73''$. Each fiber has an active core diameter of $4''.69$ ($500 \mu\text{m}$); cladding and a buffer increase the total fiber diameter to $5''.6$. The filling factor for the grid is $\sim 25\%$ on average, but rises to $\sim 55\%$ in the inner $16''$, where the fibers are more densely packed. In addition to the 75 fibers arranged in a square, another seven fibers are spaced around the square, roughly $70''$ – $90''$ from the center, and are used to measure the “sky” flux. An example of the SparsePak footprint is shown in Figure 1.

SparsePak feeds the WIYN Bench Spectrograph, a fiber-fed spectrograph designed to provide low-to-medium-resolution spectra. We used the Bench Spectrograph camera (BSC) and 316 lines mm^{-1} echelle grating in order to cover $6500 \text{ \AA} < \lambda < 6900 \text{ \AA}$, with a dispersion of $0.2 \text{ \AA pixel}^{-1}$ ($8.8 \text{ km s}^{-1} \text{ pixel}^{-1}$) and an instrumental FWHM of 0.6 \AA

(26.5 km s^{-1}). The BSC images the spectrograph onto a T2KC thinned SITE 2048×2048 CCD with $24 \mu\text{m}$ pixels. The chip has a read noise of $4.3 e^-$ and was used with the standard gain of $1.7 e^- \text{ ADU}^{-1}$. The peak system throughput for this setup is roughly 5.5% , estimated from standard-star observations (M. A. Bershad, D. R. Andersen, & M. V. Verheijen 2003b, in preparation).

Given SparsePak’s $\sim 15''$ center-to-center fiber spacing and total area, we used three pointings along the galaxy’s position angle to maximize spatial coverage and filling factor. Typical pointing offsets were $\sim 6''$. The observed galaxies have moderate sizes ($a \sim 2.0$), and their velocity field can thus be mapped from center to edge. Total SparsePak integrations consisted of three pointings with two 900 s exposures per pointing, for a total of 1.75 hr per galaxy. Multiple exposures at each position were used to identify and remove cosmic rays.

Spectra obtained from SparsePak closely resemble WIYN Densepak or Hydra spectra (i.e., multifiber spectral data). Thus, basic spectral extraction, flattening, wavelength calibration, and sky subtraction were done with the NOAO IRAF⁴ package *dohydra*. After basic reductions, we used a Gaussian line-fitting algorithm to measure Gaussian fluxes, widths, centers, and centroid errors for $H\alpha$ emission lines (D. R. Andersen et al. 2003, in preparation). We rejected any line with a signal-to-noise ratio (S/N) less than 5. More than 70% of measured $H\alpha$ lines, even at the edge of the field, had significantly higher S/Ns, with $S/N \gtrsim 20$, yielding a mean centroiding error of only 2.4 km s^{-1} for these 15 galaxies.

The V and I images were acquired at the WIYN 0.9 m telescope in $f/13.5$ mode ($0''.43 \text{ pixel}^{-1}$); integrations were 600 s in each filter. Isophotal brightness errors are $\lesssim 0.1 \text{ mag arcsec}^{-2}$ at, or below, $26.5 \text{ mag arcsec}^{-2}$ in V and I . The imaging was obtained in nonphotometric conditions (thin wisps covered the Arizona desert sky) and thus cannot readily be merged into the Shellflow imaging database.

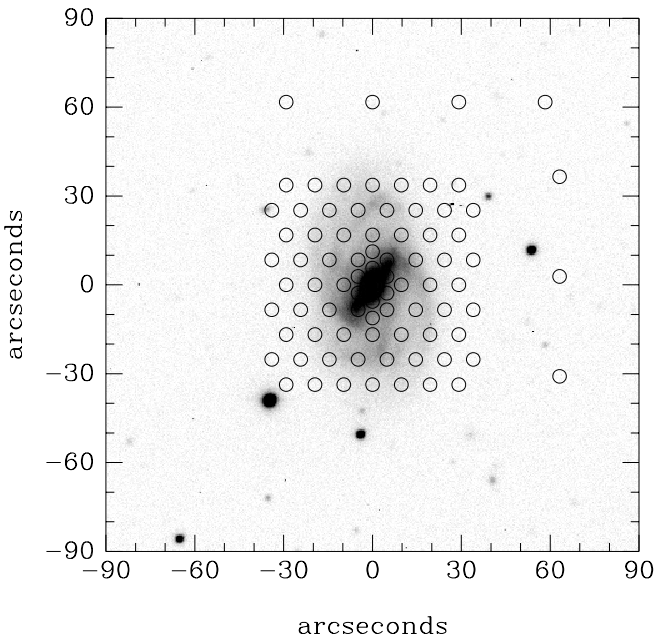


Fig. 1.—SparsePak fiber footprint for one pointing overlaid on our CCD I -band image for the SBbc galaxy UGC 5141.

⁴ IRAF is distributed by the NOAO, which is operated by AURA, Inc., under cooperative agreement with the National Science Foundation.

Structural parameters can still be measured accurately, down to deep levels, as we discuss below.

Three previously observed SB (NGC 2540, UGC 5141, and UGC 8229) and two SAB (NGC 3029 and UGC 6895) Shellflow galaxies with available long-slit H α spectra and V, I photometry were duplicated at the WIYN telescopes for comparison. These observations enable us to tie the SparsePak velocity field information to the Shellflow long-slit spectra obtained with the KPNO and CTIO 4 m telescopes+RC Spec (S. Courteau et al. 2003b, in preparation).

2.2. Data Analysis

Azimuthally averaged surface brightness profiles were extracted for all the galaxies, using ellipse fitting with a fixed center. To ensure a homogeneous computation of structural parameters and color gradients, we use the position angles and ellipticities of our I -band isophotal maps to determine the surface brightness profiles in the V band. The position angle and ellipticity are allowed to vary at each isophote. Please refer to Courteau (1996) for details about our surface brightness extraction technique.

Reduction techniques for the extraction of RCs from long-slit spectra are described in Courteau (1997). We simply state here that the one-dimensional RC is constructed by measuring an intensity-weighted centroid at each resolved major-axis H α emission feature above a noise threshold. For the two-dimensional SparsePak data, a single, inclined, differentially rotating, circular disk model with a fixed center is used to fit the H α velocity fields (D. R. Andersen & M. A. Bershadsky 2003, in preparation). Briefly, we assume a radially symmetric RC and an axisymmetric velocity field. Using this smooth functional representation of the velocity field, we compared the model velocity field to observations. Parameters are varied using a multi-dimensional downhill simplex method (Press et al. 1992) to minimize a χ^2 statistic. Our velocity field model has nine free parameters: seven for the RC (see next paragraph) and two for inclination and position angle. Two additional parameters account for positional offsets from differential telescope pointing errors for each SparsePak position, yet in practice these parameters were consistent with zero and were thereafter not allowed to vary.

We parameterize the model used to fit the RCs of both the one-dimensional (long-slit) and two-dimensional (SparsePak) velocity field data with the following empirical function:

$$v(r) = v_0 + v_a \frac{(1+x)^\beta}{(1+x^\gamma)^{1/\gamma}} \quad (1)$$

(Courteau 1997), where $x = 1/R = r_t/(r - r_0)$, v_0 and r_0 are the velocity and spatial centers of rotation, respectively, v_a is an asymptotic velocity, and r_t is a transition radius between the rising and flat parts of the RC. Solid-body rotation, or $v(r) \propto r$ (with $\partial v/\partial r \sim v_a/r_t$), is recovered for $|r - r_0| \ll r_t$, and flat rotation, or $v(r) \propto v_a$, is achieved for $|r - r_0| \gg r_t$. The term γ governs the degree of sharpness of turnover, and β can be used to model the drop-off or steady rise of the outer part of the RC.

Table 1 gives velocity field and structural parameters for the SparsePak data collected at WIYN in 2002 March. Listed are the number N of velocity data points, the kinematic and photometric inclinations, the kinematic and

photometric position angles, the velocity fit parameters v_a , r_t , β , and γ (see eq. [1]), the bar radius R_{bar} in the plane of the galaxy, the I -band scale length h of the disk, and the recessional velocity of the galaxy, v_0 . The bar radius is defined as the location where the I -band surface brightness drops and/or position angle changes abruptly. Disk scale lengths were determined as in MacArthur et al. (2003). No photometric parameters are listed for IC 0784, which could not be observed at the telescope because of time and weather constraints.

The Appendix contains RCs, extracted velocity fields (spider diagrams), and I -band images (see Figs. 7–21) for the WIYN/SparsePak galaxies. The model RCs, based on equation (1), are a decent match to most extracted integral field velocity data points. These models are shown mostly for illustrative purposes and for comparison with similar fits to RCs derived from long-slit spectra. They can also be used for future dynamical modeling.

The overall impression from the comparison of velocity data for the five Shellflow galaxies with long-slit one-dimensional and SparsePak two-dimensional RCs in the Appendix is very favorable. For NGC 2540 (Fig. 9), the one- and two-dimensional velocity models are indistinguishable, owing in part to the very similar position angles and inclinations used to extract the velocity amplitudes. The unbarred galaxy, NGC 3029 (Fig. 10), was reobserved for a consistency check; again the velocity data and models agree very well within the measurement uncertainty. NGC 5141 (Fig. 17) shows only slight differences in the modeled RCs, and UGC 6895 (Fig. 18) and UGC 8229 (Fig. 20) show slightly larger differences in the inner slopes, perhaps caused by a misaligned slit. While the data distributions agree within their respective scatter, the RC models predict different maximum rotation speeds, at the 10–20 km s $^{-1}$ level. However, the basic impression to retain for this comparison is that long-slit and IFS RCs agree well within their measurement errors and intrinsic scatter, and it can be assumed that line widths from one-dimensional RCs are a fair representation of the overall velocity field, even for barred galaxies. Close agreement between one-dimensional RCs from H α long-slit spectra and major-axis RCs from Fabry-Pérot (two-dimensional) velocity fields was also demonstrated by Courteau (1997).

Another concern, when mapping the kinematic and dynamic structure of barred galaxies, is whether our diagnostics are affected by noncircular velocities, radial flows, and/or isophotal distortions. In order to assess the importance of noncircular motions, we have examined minor-axis RCs (not shown here, for simplicity) and spider diagrams in the Appendix (see also Swaters et al. 2003). The minor-axis RCs are consistent with 10–20 km s $^{-1}$ velocity dispersions of the turbulent gas, with little hint of systematic deviations. The spider diagrams do show signs of noncircular motions, especially within $\sim 1.2R_{\text{bar}}$ ($\simeq 1.5h_{\text{disk}}$). However, beyond the extent, or reach, of the bar, most position-velocity diagrams are symmetric about the major kinematic axis. With the exception of IC 2104 (Fig. 8), a symmetric velocity pattern is recovered for all galaxies at, and beyond, R_{disk} .

The good match between one- and two-dimensional velocity fields and lack of significant noncircular motions at or beyond R_{disk} suggest that we can compare raw rotation speeds of barred and unbarred galaxies, all other quantities being equal, without significant bias. This is what we do in § 3 for the Shellflow and SCII data. Any putative offset of

the barred galaxies in the TF plane should not be due to systematic effects in the line widths.

Deprojection of velocity fields requires an inclination estimate. TF studies usually make use of photometric inclinations determined in the outer disk, away from a bar or spiral distortions, where ellipticities and position angles do not vary appreciably (see, e.g., Courteau 1996; Beauvais & Bothun 2001). We compare our SparsePak kinematic and I -band photometric inclination and position angle estimates in Figure 2 and Table 1. A position angle offset would systematically lower the observed long-slit rotation, and inclination differences could displace a galaxy in the TF plane. We find that galaxies with $i_{\text{kin}} > 45^\circ$ show no appreciable inclination offset (within 3° rms) and a mild position angle offset (10° rms) between kinematic and photometric estimates. Position angle differences can be large for more face-on galaxies, but our sample is too small to isolate systematic trends.

For galaxies with $i < 35^\circ$, photometric inclination angles are, on average, $\sim 12\%$ larger (more edge-on) than kinematic estimates. Inclination offsets for the low-inclination unbarred galaxy NGC 3029 are large and can only be explained by model-fitting (kinematic vs. isophotal) differences, whereas excellent agreement is found for UGC 6895, a higher inclination ($i = 45^\circ$) unbarred galaxy.

Note that our velocity model assumes circular, instead of elliptical, orbits. Kinematic inclinations are still precise enough to construct a TFR with small scatter ($\sigma_{\text{TF}} \simeq 0^{\text{m}} 3$), even at very low inclinations (D. R. Andersen & M. A. Bershadsky 2003, in preparation). It is, however, unclear whether the kinematic or the photometric inclination is more “representative” of the disk projection on the sky. The inclination offset may result from a combination of kinematic modeling that favors more circular orbits and great sensitivity of the isophotal mapping technique to $m = 2$ brightness perturbations. Spiral arms typically

originate at the ends (inner Lindblad resonance) of bars and retain a small pitch angle, highly noticeable in the brightness distribution, hence the plausible bias toward higher photometric inclinations. These effects are especially acute when spiral arms are fully resolved.

In a similar study, Sakai et al. (2000; H_0 Key Project) find that photometric and kinematic (radio synthesis mapping) inclination angles differ for barred galaxies. Among the 21 calibrator galaxies in their TF sample, seven are barred, and their kinematic inclination angles are $\sim 10\%$ – 15% smaller than photometric inclinations. Their barred galaxies all have $i_{\text{phot}} > 45^\circ$. However, inclination offsets for their unbarred galaxies are nearly absent. Peletier & Willner (1991) give radio and infrared inclination angles for 13 barred and unbarred nearby spirals with $27^\circ < i < 70^\circ$. Radio synthesis inclinations are also $\sim 12^\circ$ smaller than photometric estimates, but for all inclinations.

To illustrate this potentially confusing situation, we plot in Figure 3 the inclination difference, Δi (kinematic minus photometric), against kinematic inclination for the galaxy samples considered above, plus a sample of nearby, face-on, unbarred spiral galaxies (Andersen 2001). At low inclinations, kinematic inclinations appear to be systematically lower (more face-on) than photometric inclinations, with a trend of increasing differences with decreasing inclination. This is made very clear by examination of Andersen’s data. At high inclinations, both barred and unbarred galaxies have smaller inclination offsets, apparently independent of inclination. At these high inclinations, the effect on the velocity deprojection is negligible ($< 5\%$). It may be that SparsePak and photometric inclinations in these inclined galaxies are affected by extinction, as higher opacity would naturally bias high optically determined inclinations. However, the radio

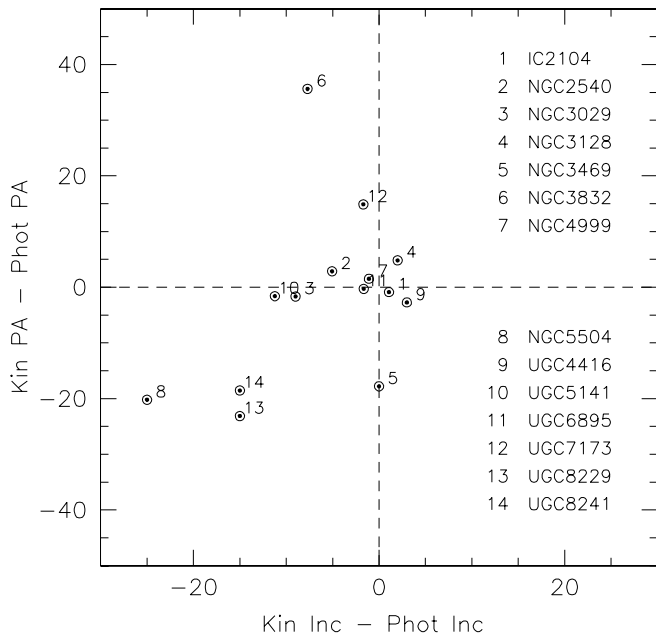


Fig. 2.—Differences in measurements of kinematic and photometric position angles and inclinations for galaxies with available two-dimensional velocity fields and I -band imaging. Inclination differences are larger for progressively face-on orientations.

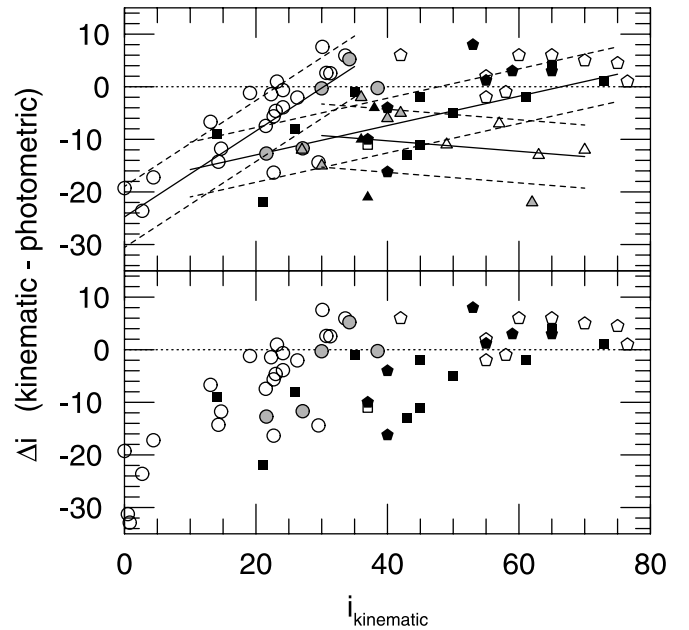


Fig. 3.—Difference between kinematic and photometric inclinations vs. kinematic inclination for four galaxy samples. The symbols are for this study (squares), Andersen (2001; circles), Peletier & Willner (1991; triangles), and Sakai et al. (2000; pentagons). Open, gray, and black symbols represent unbarred, weakly barred, and strongly barred galaxies, respectively. The top panel shows simple regressions to the Courteau et al. (this study), Andersen, and Peletier & Willner samples (independently). We exclude the Peletier & Willner sample in the bottom panel.

synthesis inclinations compiled in Sakai et al. (2000) are insensitive to dust, and the inclination difference is most likely explained by modeling differences; two-dimensional velocity fields are modeled under the assumption of circular orbits, and the larger kinematic inclinations at large inclination may result from an underestimate of the disk thickness. In general, with increasing inclination, photometric inclinations become increasingly sensitive to the estimated disk thickness, while velocity fields (especially radio velocity fields) become increasingly affected by warps and other non-circular motions. In any event, the inclination differences at $i_{\text{kin}} > 50^\circ$ are small ($< 5^\circ$) and do not affect our study. Barnes & Sellwood (2003) find a similar result for a sample of inclined galaxies with inferred photometric and kinematic (Fabry-Pérot) inclinations.

Opposite trends are found in the compilation of Peletier & Willner (1991), if all their data are considered. Inclination offsets are large even at high inclinations. This discrepancy, however, hinges on three galaxies, NGC 4178, 4192, and 4216, that display various pathologies. NGC 4178 is a very late type system, NGC 4192 has a strong warp in the outer disk, and NGC 4216 has a very pronounced dust lane; these all make photometric measurements uncertain. If we ignore the Peletier & Willner data (bottom panel of Fig. 3), we find that the transition threshold at which kinematic inclinations becomes significantly lower than photometric inclinations depends on type: $i_{\text{kin}} = 50^\circ$, 40° , and 30° for barred, weakly barred, and unbarred galaxies, respectively.

Clearly, a more extensive two-dimensional spectroscopic survey of barred and unbarred galaxies in the near-infrared and radio will help address our general concerns about their dynamical structure and the limitations of our modeling techniques. Infrared imaging should also be secured for extinction-free inclination measurements. The measurement of a “true” inclination of a galaxy is certainly ill defined, as it depends on the bandpass, dust extinction, detector, reduction methods, and assumptions concerning the galaxy structure (e.g., the presence of warps). Yet inclination angles from radio synthesis mapping may come closest to the most representative tilt angle of a galaxy on the sky.

As we await more detailed comparisons of radio and optically determined inclinations, systematic differences between barred and unbarred galaxies can be avoided if we restrict our Shellflow and SCII samples to galaxies with $i_{\text{phot}} \gtrsim 50^\circ$. Fortunately, all barred galaxies in our samples (Shellflow and SCII) already meet this criterion. We pursue our TF analysis with a discussion of Shellflow and SCII galaxies below. Our SparsePak sample will be reconsidered for TF analysis when calibrated imaging is available.

3. THE TFR OF BARRED GALAXIES

We use the Shellflow and SCII all-sky TF surveys to map the location of barred galaxies in the TF plane. Shellflow includes 300 bright spiral (Sab–Scd) field galaxies in a shell bounded at $4500 \text{ km s}^{-1} < cz < 7000 \text{ km s}^{-1}$, and SCII has 441 cluster spiral galaxies (Sa–Sd) spanning $5000 \text{ km s}^{-1} < cz < 19000 \text{ km s}^{-1}$.

Shellflow galaxies were drawn from the Optical Redshift Survey sample of Santiago et al. (1995) with inclinations in the range 45° – 78° , $m_B \leq 14.5$, and $|b| \geq 20^\circ$. Interacting, disturbed, and some barred galaxies were rejected. Rotation speeds from resolved $H\alpha$ RCs were measured at 2.2 disk scale lengths; the upper inclination limit ($i < 78^\circ$) reflects a

desire to minimize extinction effects in the inner parts of the RC (see, e.g., Courteau & Faber 1988; Giovanelli & Haynes 2002). Deep I - and V -band images were collected for each Shellflow galaxy. Disk scale lengths were obtained from bulge-to-disk (B/D) decompositions of the azimuthally averaged I -band surface brightness profile (S. Courteau et al. 2003b, in preparation).

The SCII cluster galaxies were selected from CCD I -band images taken at the KPNO and CTIO 0.9 m telescopes and classified by eye and by their B/D ratio or concentration index. These galaxies have inclinations in the range 32° – 90° and I -band magnitudes $12 \leq m_I \leq 17$. SCII line widths were measured from both $H\alpha$ long-slit spectra and $H\text{ I}$ line profiles. SCII disk scale lengths were obtained by “marking the disk,” or fitting the exponential part of the SB profile from ~ 21 to $\sim 25 I \text{ mag arcsec}^{-2}$ (Dale et al. 1999).

Shellflow and SCII galaxies have $-20 \leq M_I^{\text{Shell}} \leq -24$ and $-18 \leq M_I^{\text{SCII}} \leq -24$, respectively. Both TF calibrations are based on digital I -band imaging; $V-I$ colors, to test for M/L ratio variations and extinction effects, are available for the Shellflow sample only. Deprojection of velocity widths uses photometric inclinations measured in the outer disk, where ellipticities and position angles do not vary appreciably. Shellflow and SCII magnitudes are corrected for Galactic and internal extinction, and distances account for a Hubble expansion, a bulk flow model, and effects of incompleteness. The exact choice of distance scale does not affect our conclusions.

According to the RC3 (de Vaucouleurs et al. 1991), 37% of the Shellflow sample is barred (SB types only). In general, the proportion of galaxies with bars of all sizes is even higher (Eskridge et al. 2002), but we are here only concerned with galaxies with the strongest bars, i.e., those with potentially the highest central baryon fraction. Visual examination of the Shellflow galaxies revealed only six strongly barred systems (at I band); these have $R_{\text{bar}}/h_{\text{disk}} \geq 1.2$, where R_{bar} and h_{disk} are the size of the bar semimajor axis and disk scale length, respectively. Visual examination of the SCII galaxies yielded 27 strongly barred galaxies (D. Dale 2002, private communication). In both samples, only barred galaxies with $M_I \leq -20.4$ could be identified. The Shellflow and SCII subsamples of barred galaxies are by no means complete, nor are the parent catalogs, and a significant number of bars will be missed, especially at low magnitudes and high inclinations, where morphological identification becomes problematic.

Figures 4 and 5 show the distributions of rotational velocities and exponential scale lengths versus I -band absolute magnitudes for Shellflow and SCII galaxies. Different symbols identify the full range of spiral Hubble types; barred galaxies are further emphasized as filled symbols with open circles. Looking at the top panel of Figure 4 for Shellflow galaxies, one sees a small offset of barred galaxies from the mean TFR, consistent with these galaxies being systematically brighter for a given mass (line width). The same statistically loose trend for barred galaxies was observed by Sakai et al. (2000). It could be explained if barred galaxies have higher star formation rates. However, Phillips (1996) and Kennicutt (1998) find that global star formation rates in barred and unbarred galaxies of the same Hubble type are comparable. The TF offset, if real, might also be consistent with maximal disks being brighter than their dark matter-dominated counterparts at a given mass.

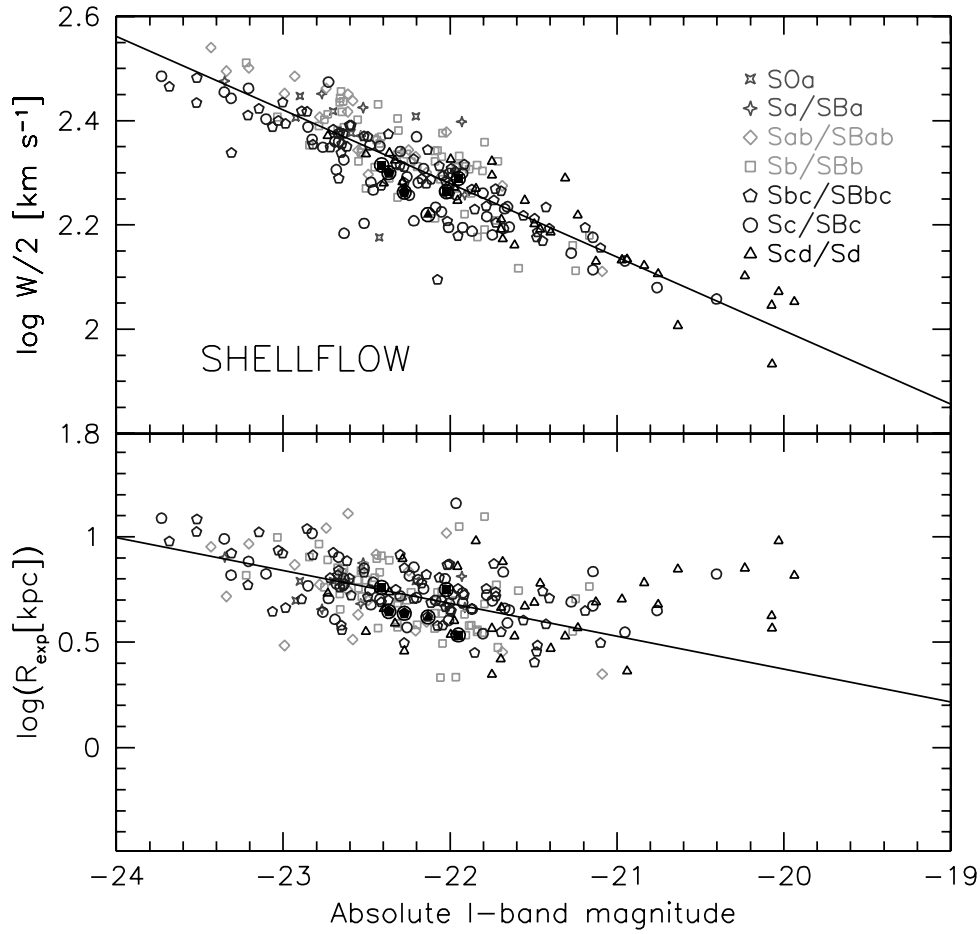


FIG. 4.—Line width–luminosity (*top*) and size–luminosity (*bottom*) diagrams for Shellflow galaxies. Line widths are measured at 2.2 disk scale lengths, and disk scale lengths are obtained from B/D decompositions of the surface brightness profile. Barred galaxies have filled symbols consistent with their Hubble type and are further emphasized with an open circle. Barred galaxies lie below the mean TFR, appearing to be systematically brighter for their rotational velocity. As in Sakai et al. (2000), this is a small-number artifact. The solid line shows a fit from our data-minus-model minimization technique (S. Courteau et al. 2003a, in preparation). [See the electronic edition of the *Journal* for a color version of this figure.]

A clearer picture is obtained with the larger SCII sample (Fig. 5), which shows no offset from the mean TFR for SCII barred galaxies. The combined velocity offset for the Shellflow and SCII barred galaxies in the two samples is $\langle \delta \log V \rangle = -0.02 \pm 0.04$, consistent with no deviation of the mean TFR. Note that photometric inclinations are used to deproject velocities in Shellflow and SCII, but using kinematic inclinations instead would simply imply a readjustment of the TF zero point. Provided that only one inclination measure is used, the relative distribution of barred and unbarred TF galaxies is not affected by the precise choice of inclination (§ 2.2). Recall that all the Shellflow and SCII barred galaxies have $i > 50^\circ$ and are not affected by a putative (kinematic minus photometric) inclination offset. Furthermore, if we exclude the few unbarred galaxies that have $i < 50^\circ$ from the Shellflow and SCII samples, the TF distributions remain the same. Thus, we conclude that *barred galaxies lie on the same TFR as unbarred galaxies*. A similar realization was also reached by DS00.

The kinship between barred and unbarred galaxies extends to other properties as well. The lower panels of Figures 4 and 5 show no statistical differences in the scale lengths of barred and unbarred galaxies (for a given absolute magnitude). Figure 6 shows the color–magnitude

diagram of Shellflow galaxies. Notwithstanding small statistics, barred and unbarred galaxies have similar colors, consistent with their having comparable star formation rates (Kennicutt 1998). MacArthur et al. (2003) find other similarities for structural parameters of barred and unbarred galaxies: their bar/bulge light profiles are close to exponential, and their ratio of bulge effective radius, r_e , and disk exponential scale length, h , falls in the range $r_e/h = 0.22 \pm 0.09$, expected for late Freeman type I spiral galaxies.

CR99 developed and applied a test for correlated scatter of the TFR. According to this test, pure stellar exponential (maximal) disks should deviate from the mean TF and luminosity–size (LS) relations in such a way that $\partial \log V_{\text{disk}} / \partial \log R_{\text{exp}} = -0.5$. Thus, strongly correlated TF/LS residuals for the barred spirals would support the suggestion that unbarred spirals have submaximal disks (high-concentration halos) and that maximal disks are only found, on average, in barred spiral galaxies. A new analysis based on the Shellflow and SCII data sets yields residuals that are consistent with $\partial \log V_{\text{disk}} / \partial \log R_{\text{exp}} = 0.0$ for both barred and unbarred galaxies. CR99 found a similar result for the Courteau–Faber (1988; also see Courteau 1996, 1997) sample. This result further confirms earlier

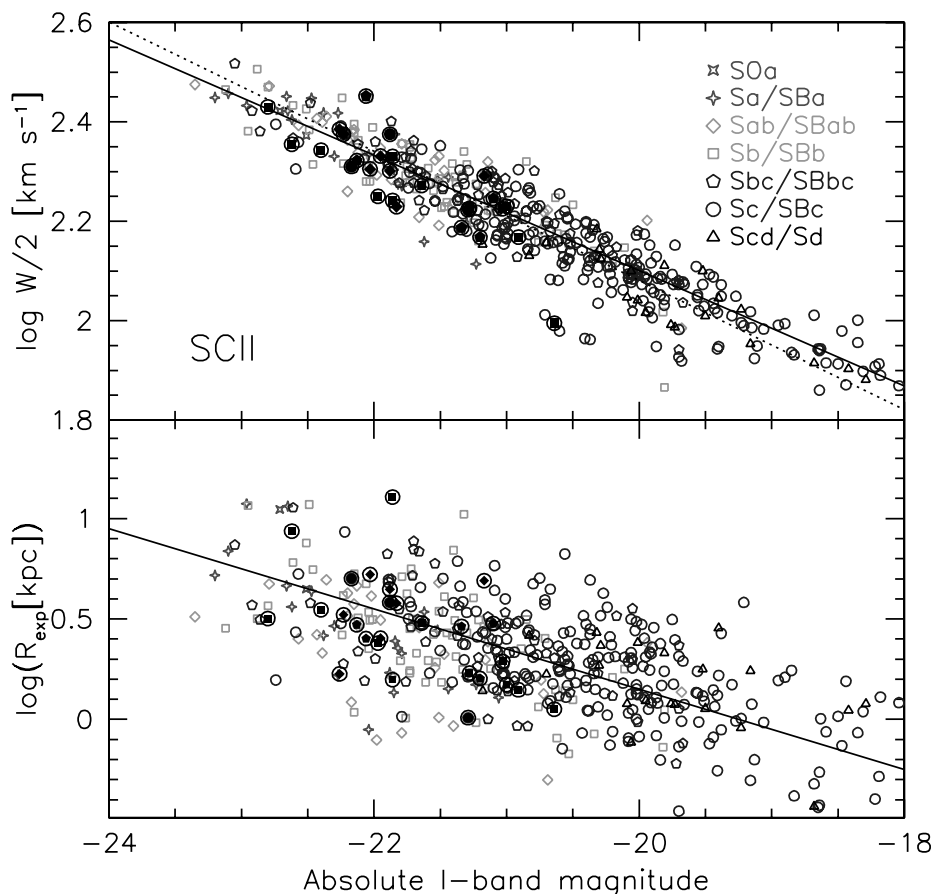


FIG. 5.—Line width–luminosity (*top*) and size–luminosity (*bottom*) diagrams for SCII galaxies. Line widths are measured from $H\alpha$ RCs and $H\text{I}$ line widths, and disk scale lengths are measured using the marking-the-disk technique (see text). Symbols are as in Fig. 4. The TFR is the same for barred and unbarred galaxies. The solid and dashed lines show data-minus-model minimization fits from S. Courteau et al. (2003a, in preparation) and Dale et al. (1999), respectively. [See the electronic edition of the *Journal* for a color version of this figure.]

observations about spiral galaxies: barred and unbarred galaxies have similar physical properties and populate the same TF/LS relation and residual space. It also shows that the TFR is fully independent of surface brightness (CR99), a situation that may also result from the fine-tuning of virial parameters. The analysis of the independence of surface brightness in the TFR, and a revised interpretation of the “Courteau-Rix” test in terms of virial parameter correlations, is presented in S. Courteau et al. (2003a, in preparation).

4. DISCUSSION AND CONCLUSION

We have tested the hypothesis that barred and unbarred spiral disks have different structural correlations, such as the Tully-Fisher relation, with barred galaxies possibly having a higher luminous-to-dark matter fraction in their inner parts. New WIYN/SparsePak integral field spectroscopy and deep near-infrared photometry of barred and unbarred spiral galaxies allowed us to verify that non-circular motions are not significant at R_{disk} and that rotation curves from one- or two-dimensional spectroscopy are reliable beyond that radius. Based on this result and uniform inclination corrections for spiral galaxies with $i > 50^\circ$, we have compared the distributions of barred and unbarred galaxies in the TF plane from extensive redshift-distance surveys of galaxies and found no significant differences.

For a given circular velocity, barred and unbarred galaxies have comparable luminosities, scale lengths, colors, and star formation rates.⁵ This suggests that barred and unbarred galaxies are close members of the same family and do not originate from different evolutionary trees. Their structural duality may be understood if bars are generated by transient dynamical processes that are likely independent of the initial galaxy formation conditions. Their virial properties would otherwise be different.

Very recent N -body simulations with the highest resolution have relaxed the notion that bars would grow in structures defined by a narrow range of disk/halo parameters. Thus, our comparisons cannot be used to ascertain the notion that bars live mostly in spiral disks whose stellar fraction dominates the mass budget within the optical disk. Our results are, however, consistent with bright barred galaxies having dark matter fractions similar to those of their unbarred cousins (DS00; S. Courteau et al. 2003a, in preparation). Stellar velocity dispersions, which provide robust disk M/L ratios, hold the promise of

⁵ A comparative study by Sheth et al. (2002) of the molecular gas properties of barred and unbarred galaxies in the BIMA Survey of Nearby Galaxies shows striking differences. However, their data (see their Fig. 2) show less striking differences for the star formation rates between barred and unbarred galaxies, but based on scanty information. More data are clearly needed to elucidate these questions!

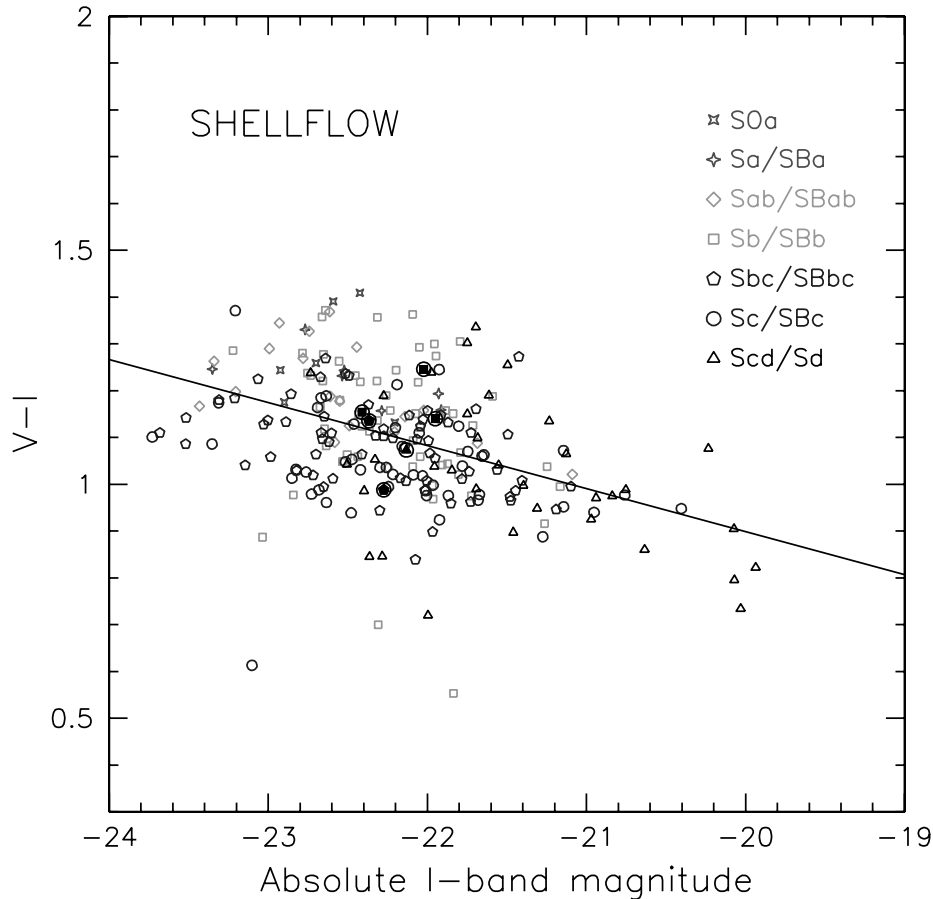


FIG. 6.—Color-magnitude diagram for Shellflow galaxies. Barred galaxies have mean colors consistent with the general spiral population. Symbols are as in Fig. 4. [See the electronic edition of the *Journal* for a color version of this figure.]

breaking the disk/halo degeneracy in mass modeling of barred and unbarred galaxies.

If the presence of bars in rotating disks is not directly related to their virial structure but rather to their local dynamical state, it can surely be used as a signpost of galaxy evolution. Given that bars may be just as important as mergers in shaping field disk galaxies, significant efforts should be invested in programs to probe differences between barred and unbarred galaxies. Bars, which can be triggered spontaneously by the global dynamical instability of a rotationally supported disk, can also be induced by interactions with a satellite. One might thus expect an *increase* of the fraction of barred disks at higher redshift, unless these younger disks are too dynamically hot to sustain bar-unstable modes. Van den Bergh et al. (2002) studied the visibility of bars in the northern Hubble Deep Field (HDF-N) and reported a *dearth* of bars at $z > 0.7$ in the rest-frame V band. Taken at face value, this could indicate a dependence of bar strength on the local galaxy density that grows with time. However, a similar study by Sheth et al. (2003) based on the NICMOS Deep Field reveals numerous strongly barred galaxies up to $z = 1.1$. Extinction effects in the bluer band explored by van den Bergh et al. (2002) thus thwarted their ability to detect dust-enshrouded bars. Given the detection of stable disks beyond $z \sim 1.3$ (van Dokkum & Stanford 2001; Genzel et al. 2003), it is thus reasonable to posit the existence of bars at comparably high redshifts. The cosmological volumes sampled in the two HDF studies

above are very small, and robust statistics on the barredness of galaxies with look-back time awaits wider coverage and more extensive sky surveys, especially with telescopes like ALMA, within the next decade.

Closer to home and on shorter timescales, our comparison of a few dozen barred galaxies with TF samples of unbarred disks should soon be superseded, it is wished, by systematic studies of structural and environmental properties of thousands of barred and unbarred galaxies in the Sloan and 2MASS galaxy catalogs. Only with such large-scale, systematic local investigations can we make significant progress in mapping galaxy evolution at high redshift and linking the near- and far-field universe.

We are grateful to Daniel Dale for information about the SCII database and to Anatoly Klypin, Jerry Sellwood, and Ben Weiner for comments about N -body simulations of barred galaxies. Constructive suggestions by the referee improved the flow of the paper. This research has made use of the NASA/IPAC extragalactic database (NED), which is operated by the Jet Propulsion Laboratory, California Institute of Technology, under contract with the National Aeronautics and Space Administration. S. C. wishes to acknowledge his colleagues on the Shellflow team (Marc Postman, David Schlegel, and Michael Strauss) for permission to use previously unpublished results. S. C. and L. A. M. acknowledge financial support from the National Science

and Engineering Council of Canada. M. A. B. acknowledges financial support from NSF grant AST 99-70780. S. C. would also like to thank the Max-

Planck-Institut für Astronomie in Heidelberg and the Max-Planck-Institut für Astrophysik in Munich for their hospitality while much of this paper was cooked up.

APPENDIX

ROTATION CURVES, VELOCITY FIELDS, AND *I*-BAND IMAGES FOR THE WIYN02 SAMPLE

This section shows long-slit (one-dimensional) and SparsePak (two-dimensional) velocity fields for all galaxies observed at WIYN in March 2002. See § 2 for details about the sample and data analysis. Shown for each galaxy in Figures 7–21 are, in the left-hand panel, the position-velocity contours (spider diagrams) superimposed on the galaxy *I*-band image and, in the right-hand panel, the SparsePak velocities (in the plane of the sky, i.e., not corrected for projection effects). The velocity data were extracted according to various techniques described in the text, and whenever available, matching RCs are shown from the Shellflow collection of long-slit spectra.

Smoothed versions of the observed velocity field were produced using the *patch* routine within the GIPSY analysis package (van der Hulst et al. 1992; Vogelaar & Terlouw 2001). The SparsePak velocity field shown in the right-hand panel is extracted from a model that includes inclination, position angle, disk center, rotation velocity, scale length, and systemic velocity. The parameterization of the velocity field is given by equation (1).

SparsePak $H\alpha$ position-velocity diagrams are constructed using two representations of the two-dimensional velocity field: The first includes all measurements with a simulated 6" "slit" for the best-fit kinematic position angle (*triangles*). The second SparsePak RC uses all measured velocities within $\pm 60^\circ$ of the kinematic major axis *in the inclined plane* of the galaxy (*squares*). Using the modeled kinematic inclination and position angle, we can project each measured rotation velocity onto the major axis. This second, "wedge," approach is relatively insensitive to inclination-induced beam smearing, which affects the simulated slit measurements. However, the wedge does not spatially sample the inner 10" as well as the slit. Our best-fit model (*solid line*) is adjusted for beam smearing induced by the $\sim 5''$ fibers of SparsePak. When comparing this model to the data, remember that the simulated slit data (*triangles*) have not been projected onto the major axis; the magnitude of these velocities serves only as a lower limit. Thus, a triangle in the center of the RC that does not have a corresponding square at the same radius implies that the center of that fiber lies more than 60° from the major axis and that its azimuth correction is large (greater than 2). The velocity models based on equation (1) trace the squares only. Further details about velocity field modeling are given in § 2.2.

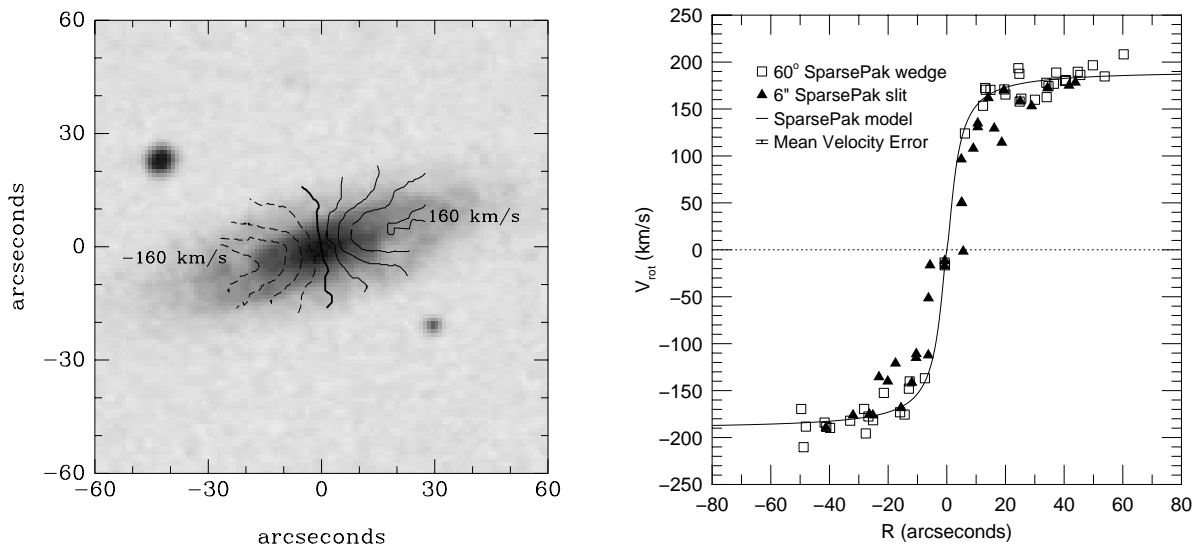


FIG. 7.—Velocity contours and *I*-band image (*left*) and RC data with velocity model (*right*) for IC 784

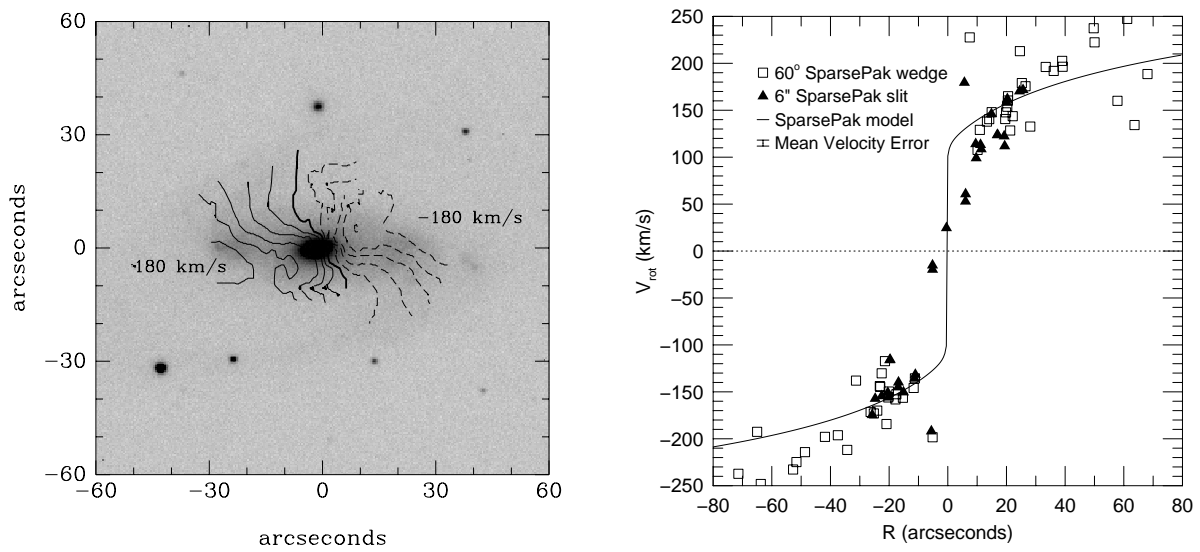


FIG. 8.—Velocity contours and *I*-band image (*left*) and RC data with velocity model (*right*) for IC 2104. This galaxy has a pathological velocity field with significant noncircular motions, a continuously rising RC, and a small inner velocity bump representative of a strong bar and/or bulge (which is poorly matched by the velocity model).

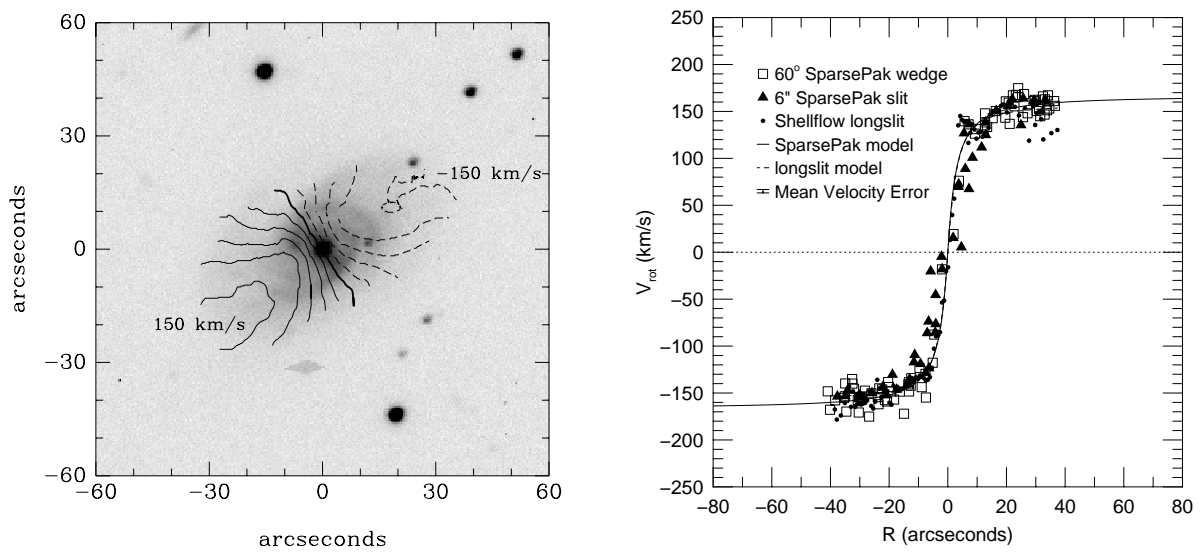


FIG. 9.—Velocity contours and *I*-band image (*left*) and RC data with velocity model (*right*) for NGC 2540

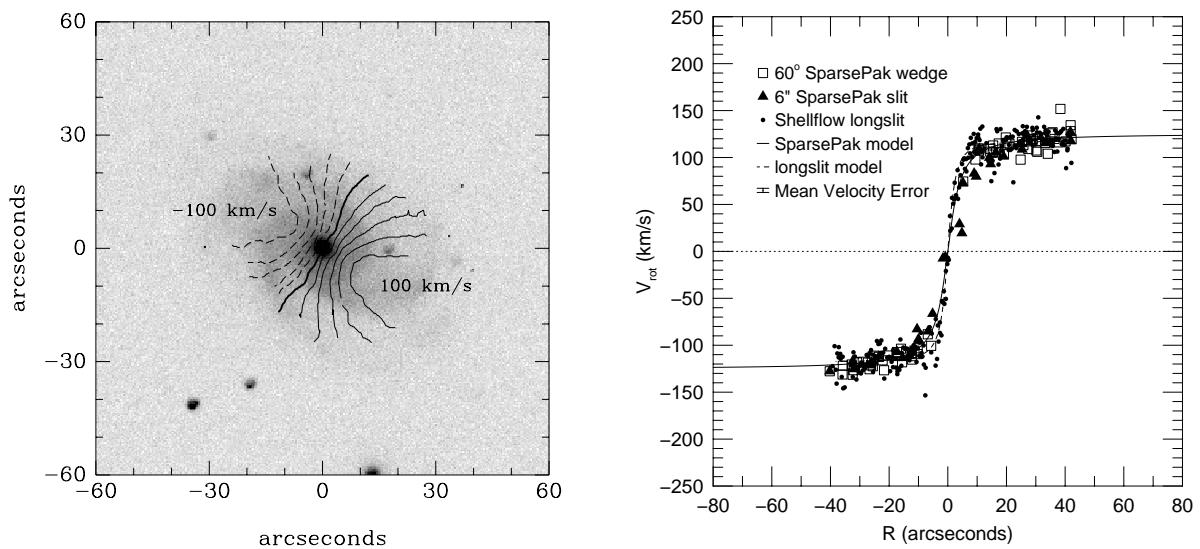


FIG. 10.—Velocity contours and *I*-band image (*left*) and RC data with velocity model (*right*) for the unbarred galaxy NGC 3029

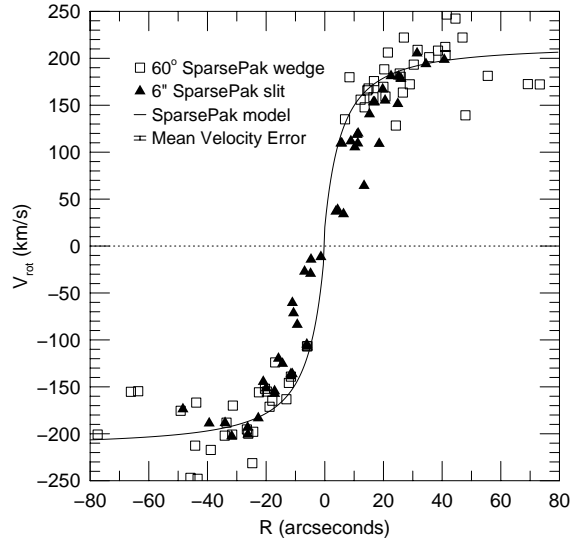
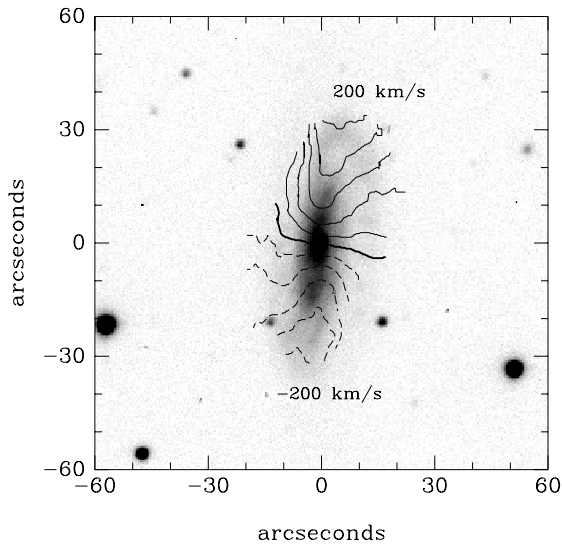


FIG. 11.—Velocity contours and *I*-band image (*left*) and RC data with velocity model (*right*) for NGC 3128

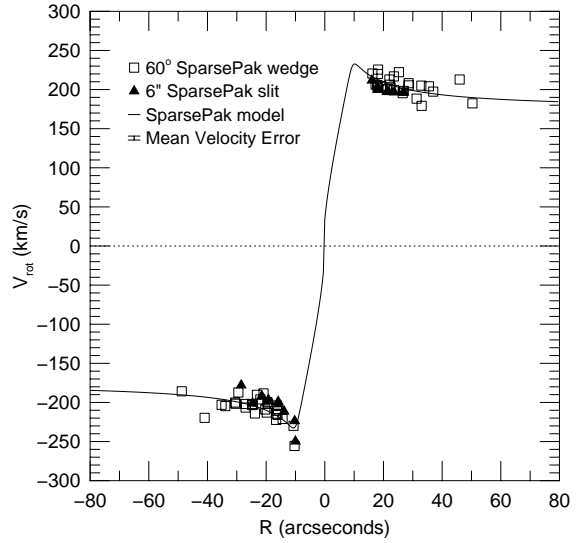
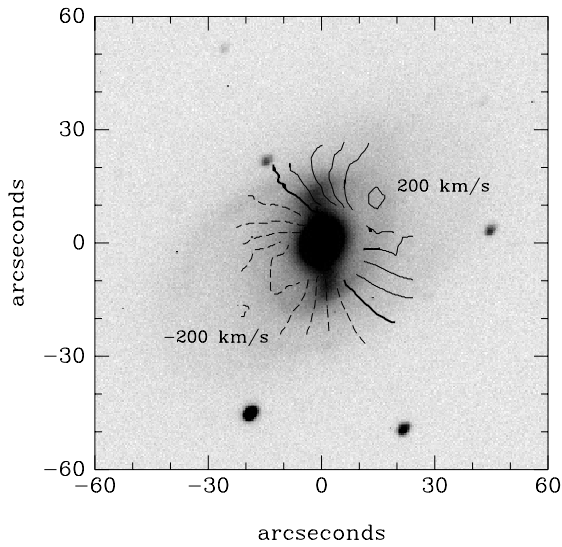


FIG. 12.—Velocity contours and *I*-band image (*left*) and RC data with velocity model (*right*) for NGC 3469

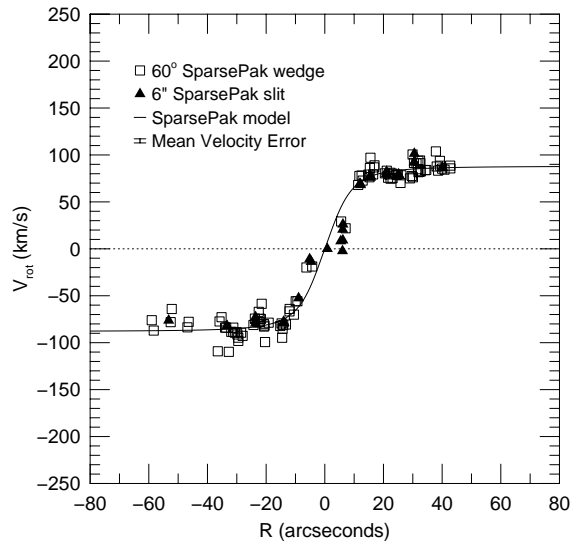
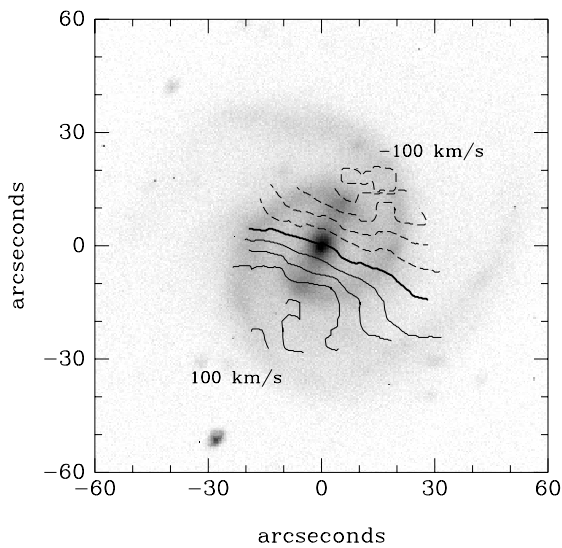


FIG. 13.—Velocity contours and *I*-band image (*left*) and RC data with velocity model (*right*) for NGC 3832

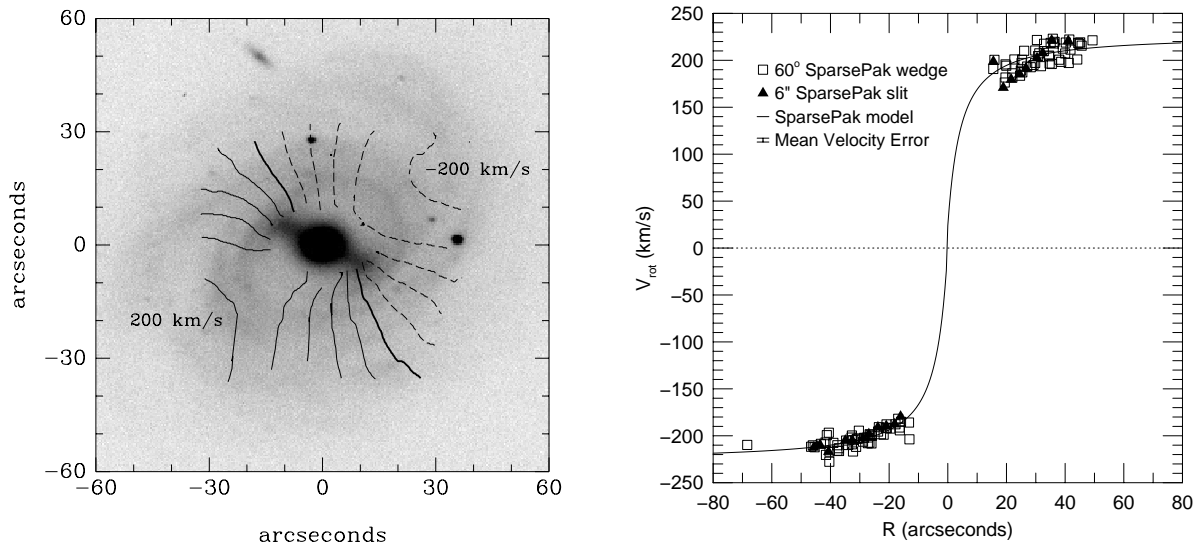


FIG. 14.—Velocity contours and *I*-band image (*left*) and RC data with velocity model (*right*) for NGC 4999

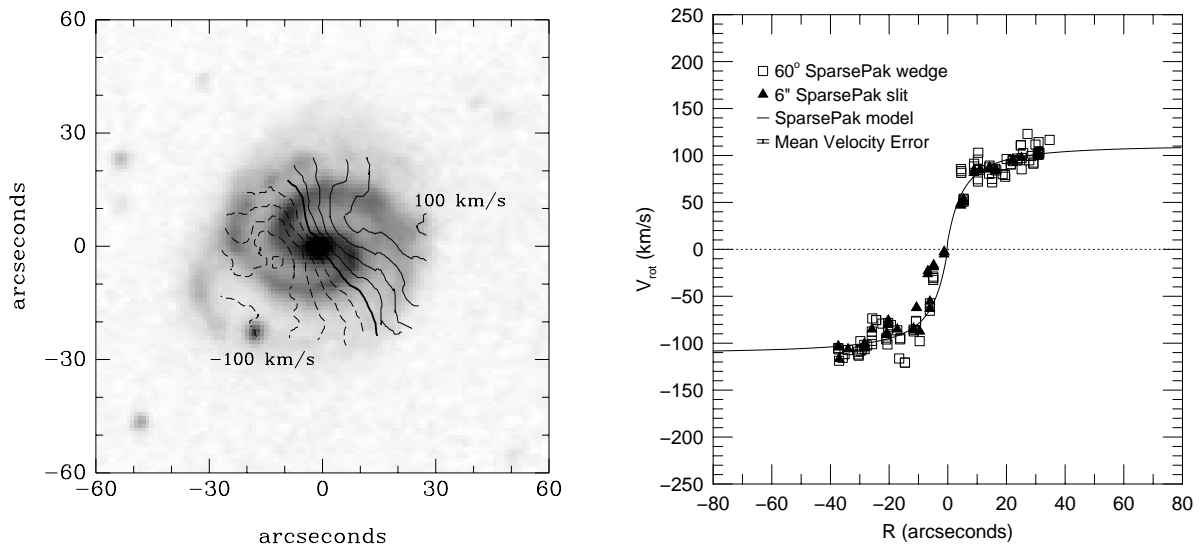


FIG. 15.—Velocity contours and Digitized Palomar Sky Survey image (*left*) and RC data with velocity model (*right*) for NGC 5504. The *I*-band image for this galaxy was not available.

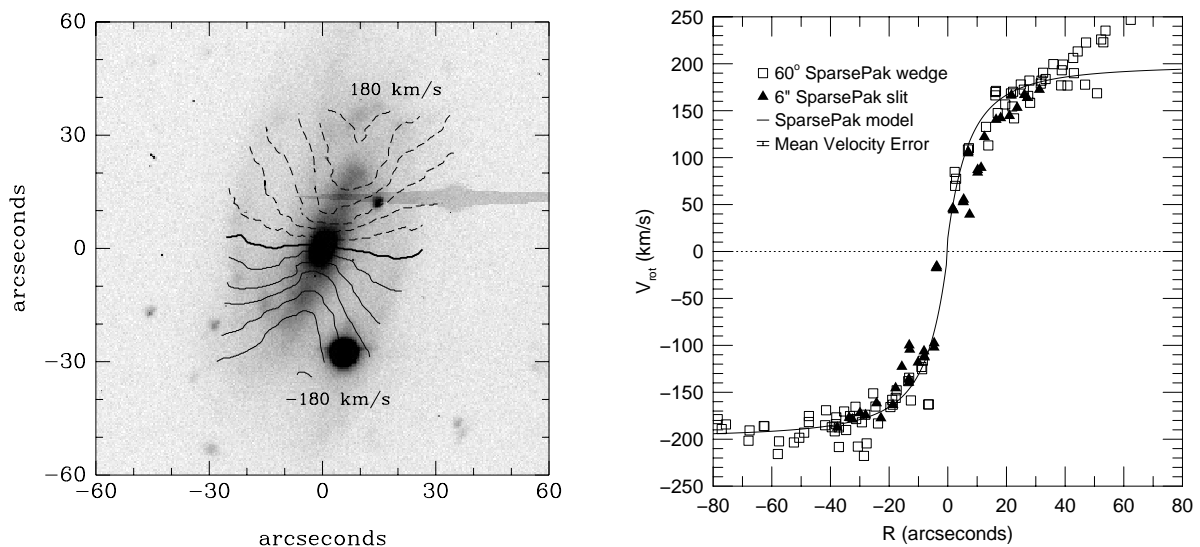


FIG. 16.—Velocity contours and *I*-band image (*left*) and RC data with velocity model (*right*) for UGC 4416. The vertical trace in the left-hand image is due to an internal reflection.

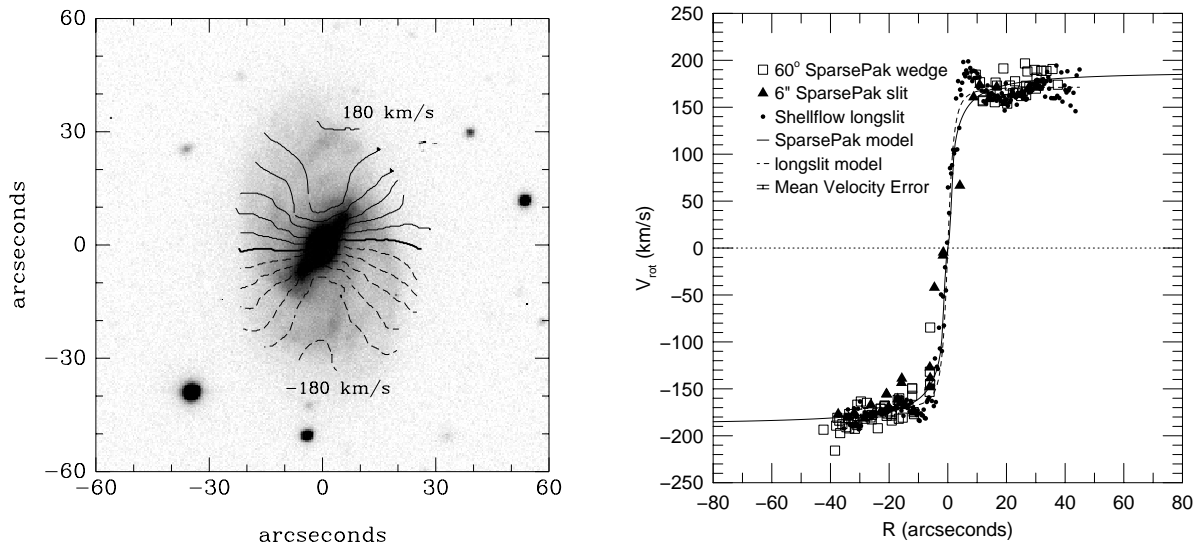


FIG. 17.—Velocity contours and *I*-band image (*left*) and RC data with velocity model (*right*) for UGC 5141

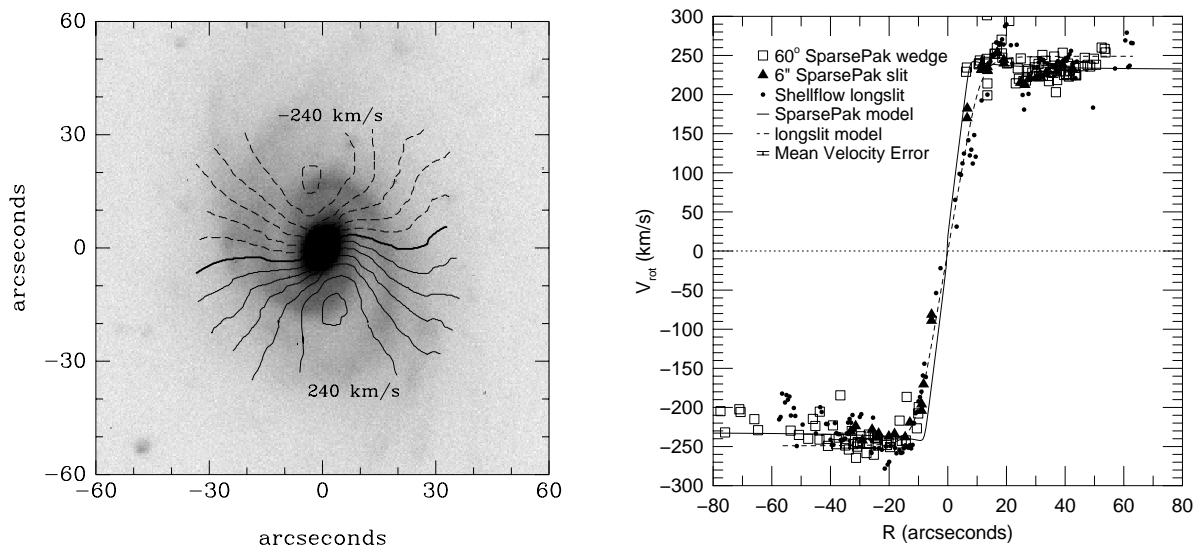


FIG. 18.—Velocity contours and *I*-band image (*left*) and RC data with velocity model (*right*) for the weakly barred galaxy UGC 6895

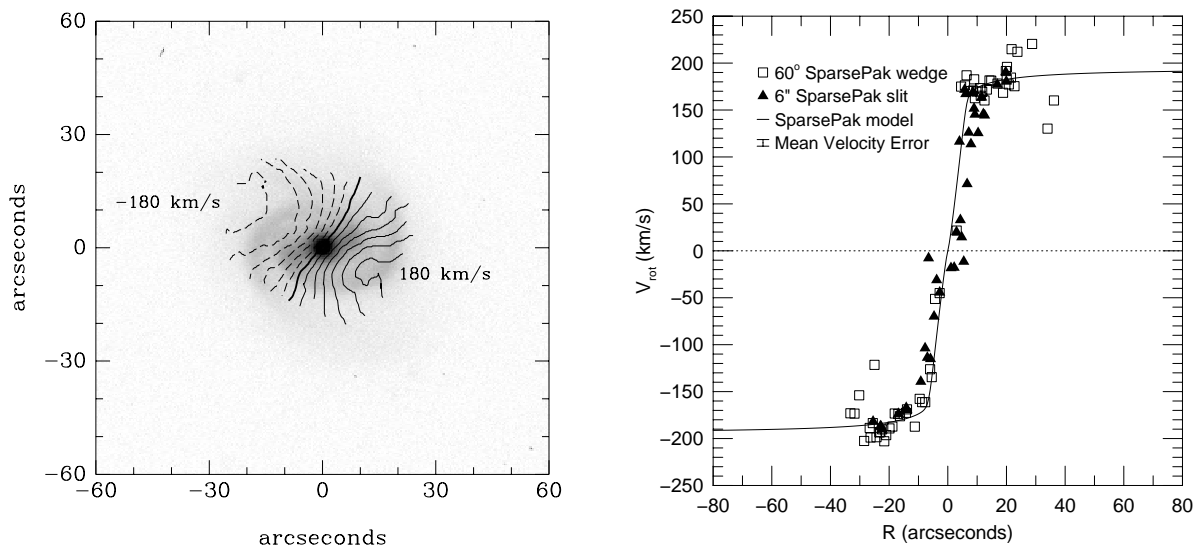
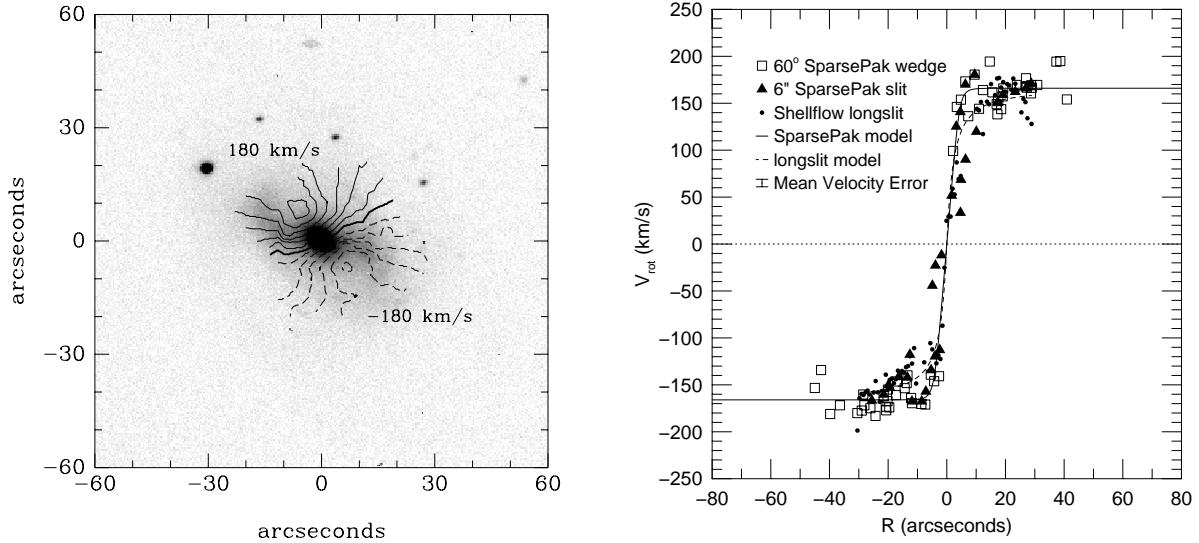
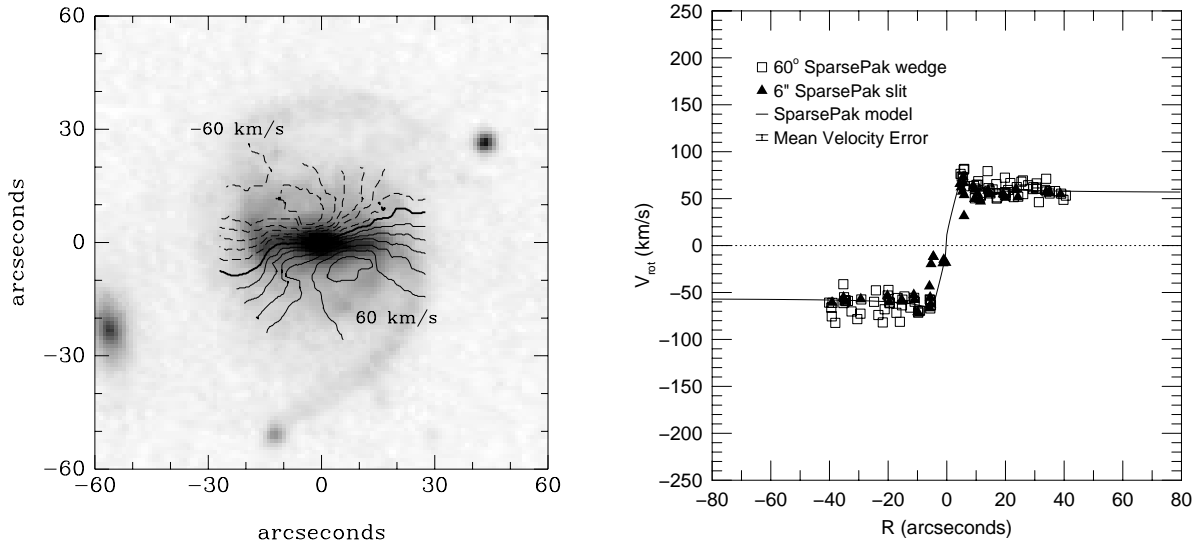


FIG. 19.—Velocity contours and *I*-band image (*left*) and RC data with velocity model (*right*) for UGC 7173

FIG. 20.—Velocity contours and *I*-band image (*left*) and RC data with velocity model (*right*) for UGC 8229FIG. 21.—Velocity contours and *I*-band image (*left*) and RC data with velocity model (*right*) for UGC 8241

REFERENCES

- Andersen, D. 2001, Ph.D. thesis, Pennsylvania State Univ.
 Athanassoula, L. 2003, MNRAS, 341, 1179
 Barnes, E. I., & Sellwood, J. A. 2003, AJ, 125, 1164
 Beauvais, C., & Bothun, G. 2001, ApJS, 136, 41
 Bell, E. F., & de Jong, R. S. 2001, ApJ, 550, 212
 Bosma, A. 1996, in ASP Conf. Ser. 91, Barred Galaxies, ed. R. Buta, D. A. Crocker, & B. G. Elmegreen (IAU Colloq. 157; San Francisco: ASP), 132
 ———. 2002, in ASP Conf. Ser. 273, The Dynamics, Structure, and History of Galaxies, ed. G. S. Da Costa & H. Jerjen (San Francisco: ASP), 223
 Bottema, R. 1997, A&A, 328, 517
 Brighenti, F., & Mathews, W. G. 1997, ApJ, 486, L83
 Broeils, A. H., & Courteau, S. 1997, in ASP Conf. Ser. 117, Dark and Visible Matter in Galaxies, ed. M. Persic & P. Salucci (San Francisco: ASP), 74
 Buchhorn, M. 1992, Ph.D. thesis, Australian National Univ.
 Buta, R., Crocker, D. A., & Elmegreen, B. G., ed. 1996, ASP Conf. Ser. 91, Barred Galaxies (IAU Colloq. 157; San Francisco: ASP)
 Ciotti, L. 2000, in ASP Conf. Ser. 197, Dynamics of Galaxies: From the Early Universe to the Present, ed. F. Combes, G. A. Mamon, & V. Charmandaris (San Francisco: ASP), 95
 Corsini, E. M., et al. 1999, A&A, 342, 671
 Courteau, S. 1996, ApJS, 103, 363
 Courteau, S. 1997, AJ, 114, 2402
 Courteau, S., & Faber, S. M. 1988, PASP, 100, 1219
 Courteau, S., & Rix, H.-W. 1999, ApJ, 513, 561 (CR99)
 Courteau, S., Willick, J. A., Strauss, M. A., Schlegel, D., & Postman, M. 2000, ApJ, 544, 636
 Dalcanton, J. J., Spergel, D. N., & Summers, F. J. 1997, ApJ, 482, 659
 Dale, D. A., Giovanelli, R., Haynes, M. P., Campusano, L. E., & Hardy, E. 1999, AJ, 118, 1489
 Debattista, V. P., & Sellwood, J. A. 1998, ApJ, 493, L5
 ———. 2000, ApJ, 543, 704 (DS00)
 Dehnen, W., & Binney, J. 1998, MNRAS, 294, 429
 de Vaucouleurs, G., de Vaucouleurs, A., Corwin, H. G., Jr., Buta, R. J., Paturel, G., & Fouqué, P. 1991, Third Reference Catalog of Bright Galaxies (New York: Springer) (RC3)
 Eskridge, P. B., et al. 2002, ApJS, 143, 73
 Fuchs, B. 2001, in Dark Matter in Astro- and Particle Physics, ed. H. V. Klapdor-Kleingrothaus (Berlin: Springer), 25
 ———. 2003, in The Evolution of Galaxies III: From Simple Approaches to Self-Consistent Models, ed. G. Hensler, G. Stasińska, S. Harfst, P. Kroupa, & C. Theis (Dordrecht: Kluwer)
 Genzel, R., Baker, A. J., Tacconi, L. J., Lutz, D., Cox, P., Guillooteau, S., & Omont, A. 2003, ApJ, 584, 633
 Gerhard, O. 2002, Space Sci. Rev., 100, 129

- Giovanelli, R., & Haynes, M. P. 2002, *ApJ*, 571, L107
- Jimenez, R., Verde, L., & Oh, S. P. 2003, *MNRAS*, 339, 243
- Kennicutt, R. C., Jr. 1998, *ARA&A*, 36, 189
- Klypin, A., Zhao, H., & Somerville, R. S. 2002, *ApJ*, 573, 597
- Kranz, T., Slyz, A., & Rix, H.-W. 2003, *ApJ*, 586, 143
- Kuijken, K. 1995, in *IAU Symp.* 164, *Stellar Populations*, ed. P. C. van der Kruit & G. Gilmore (Dordrecht: Kluwer), 195
- MacArthur, L. A., Courteau, S., & Holtzman, J. A. 2003, *ApJ*, 582, 689
- Maller, A. H., Simard, L., Guhathakurta, P., Hjorth, J., Jaunsen, A. O., Flores, R. A., & Primack, J. R. 2000, *ApJ*, 533, 194
- Mo, H. J., Mao, S., & White, S. D. M. 1998, *MNRAS*, 295, 319
- Ostriker, J. P., & Peebles, P. J. E. 1973, *ApJ*, 186, 467
- Palunas, P., & Williams, T. B. 2000, *AJ*, 120, 2884
- Peletier, R. F., & Willner, S. P. 1991, *ApJ*, 382, 382
- Phillips, A. C. 1996, in *ASP Conf. Ser.* 91, *Barred Galaxies*, ed. R. Buta, D. A. Crocker, & B. G. Elmegreen (IAU Colloq. 157; San Francisco: ASP), 44
- Press, W. H., Teukolsky, S. A., Vetterling, W. T., & Flannery, B. P. 1992, *Numerical Recipes in Fortran* (2d ed.; Cambridge: Cambridge Univ. Press)
- Sackett, P. D. 1997, *ApJ*, 483, 103
- Sakai, S., et al. 2000, *ApJ*, 529, 698
- Santiago, B. X., Strauss, M. A., Lahav, O., Davis, M., Dressler, A., & Huchra, J. P. 1995, *ApJ*, 446, 457
- Seljak, U. 2002, *MNRAS*, 334, 797
- Sellwood, J. A. 2003, *ApJ*, 587, 638
- Sellwood, J. A., & Evans, N. W. 2001, *ApJ*, 546, 176
- Sheth, K., Regan, M. W., Scoville, N. Z., & Strubbe, L. E. 2003, *ApJ*, 592, L13
- Sheth, K., Vogel, S. N., Teuben, P. J., Harris, A. I., Regan, M. W., Thornley, M. D., & Helfer, T. T. 2002, in *ASP Conf. Ser.* 275, *Disks of Galaxies: Kinematics, Dynamics and Perturbations*, ed. E. Athanassoula, A. Bosma, & R. Mujica (San Francisco: ASP), 263
- Silk, J. 2002, in *ASP Conf. Ser.* 273, *The Dynamics, Structure, and History of Galaxies*, ed. G. S. Da Costa & H. Jerjen (San Francisco: ASP), 299
- Swaters, R. A. 1999, Ph.D. thesis, Groningen Univ.
- Swaters, R. A., Madore, B. F., & Trewhella, M. 2000, *ApJ*, 531, L107
- Swaters, R. A., Verheijen, M. A. W., Bershady, M. A., & Andersen, D. R. 2003, *ApJ*, 587, L19
- Trott, C. M., & Webster, R. L. 2002, *MNRAS*, 334, 621
- Tully, R. B., & Fisher, J. R. 1977, *A&A*, 54, 661
- Valenzuela, O., & Klypin, A. 2003, preprint (astro-ph/0204028) (VK03)
- van den Bergh, S., Abraham, R. G., Whyte, L. F., Merrifield, M. R., Eskridge, P. B., Frogel, J. A., & Pogge, R. 2002, *AJ*, 123, 2913
- van der Hulst, J. M., Terlouw, J. P., Begeman, K. G., Zwitter, W., & Roelfsema, P. R. 1992, in *ASP Conf. Ser.* 25, *Astronomical Data Analysis Software and Systems I*, ed. D. M. Worrall, C. Biemesderfer, & J. Barnes (San Francisco: ASP), 131
- van Dokkum, P. G., & Stanford, S. A. 2001, *ApJ*, 562, L35
- Vogelaar, M. G. R., & Terlouw, J. P. 2001, in *ASP Conf. Ser.* 238, *Astronomical Data Analysis Software and Systems X*, ed. F. R. Harnden, Jr., F. A. Primini, & H. E. Payne (San Francisco: ASP), 358
- Weinberg, M. D., & Katz, N. 2002, *ApJ*, 580, 627
- Weiner, B. J., Sellwood, J. A., & Williams, T. B. 2001, *ApJ*, 546, 931
- Zhao, H., Rich, R. M., & Spergel, D. N. 1996, *MNRAS*, 282, 175